Available online at www.sciencedirect.com
ScienceDirect
Journal of Power Sources 168 (2007) 49–57
JOURNAL OF POWER SOURCES
www.elsevier.com/locate/jpowsour

Investigation and application of polysiloxane-based gel electrolyte in valve-regulated lead-acid battery

Zheng Tang [a], Jianming Wang [a,*], Xian-xian Mao [b], Haibo Shao [a], Quanqi Chen [a], Zhihua Xu [a], Jianqing Zhang [a,c]

[a] *Department of Chemistry, Zhejiang University, Hangzhou 310027, PR China*
[b] *Zhejiang Narada Power Source Co., Ltd., Hangzhou 310013, PR China*
[c] *Chinese State Key Laboratory for Corrosion and Protection, Shenyang 110015, PR China*

Received 1 October 2006; accepted 3 December 2006
Available online 28 December 2006

Abstract

Polysiloxane-based gel electrolyte (PBGE) is prepared and investigated as a new gel electrolyte for valve-regulated lead-acid (VRLA) batteries. PBGE particles, characterized by means of Fourier transform infrared (FTIR) spectroscopy, cyclic voltammetry (CV) and scanning electron microscopy (SEM), reveal good stability and their particle sizes are 30–50 nm. The initial cyclic properties of the absorptive glass mat (AGM)–PBGE and AGM–colloid silica gel electrolyte (CSGE) hybrid batteries are investigated by electrochemical techniques, scanning electron microscopy and X-ray diffraction (XRD). The addition of PBGE improves the utilization efficiency of positive active material (PAM) in AGM–PBGE hybrid batteries and thus enhances the batteries capacity compared with the AGM–CSGE reference batteries. Cyclic overdischarge tests show that the AGM–PBGE hybrid batteries have superior recharge and discharge during partial-state-of-charge (PSoC). It is also found that the greatly enhanced electrochemical performance of the AGM–PBGE batteries may be due to higher charge efficiency, good conductivity with lower internal resistance and the open three-dimensional network structure of the polyelectrolyte. The analysis results of SEM and XRD indicate that softening and shedding of positive active material are the main causes of failure for the two hybrid batteries.

Keywords: Polysiloxane-based gel electrolyte; Colloid silica gel electrolyte; Cycle life; Positive active material; Value-regulated lead-acid battery

1. Introduction

Two types of valve-regulated lead-acid (VRLA) battery are used, one is absorptive glass mat (AGM) technology and the other is gel technology [1]. Compared with conventional flooded or AGM batteries, gel VRLA batteries have the following features: (i) long service life and high reliability under deep-discharge cycles; (ii) no acid stratification and installation in any orientation; (iii) no leakage of acid mist, good charge stability (resistant to thermal runway), maintenance-free operation and wide operating temperature. More attention has been paid to gel VRLA batteries since the 1990s [1–14]. The key factor that affects the performance of gel batteries is the gel electrolyte itself. The most commonly used gel electrolyte [15,16] consists of fumed silica, de-ionized water and some additives. The gel electrolyte containing fumed silica has, however, many disadvantages such as short gelling time, a higher viscosity, high material and manufacture costs, as and an obvious increase of internal resistance, which limits extensive application of this technology [10].

In order to overcome the disadvantages of gel electrolyte with fumed silica, the investigation and application of colloidal silica gel electrolyte (CSGE) [10,12] have been carried out because of its good stability and low cost. High initial capacity, good high-rate discharge and high- low-temperature performance can be obtained from hybrid-VRLA batteries that integrate AGM-VRLA and gel electrolyte, and thereby exhibit both the high power density of the AGM design and the long cycle-life of normal gel batteries [12]. On the other hand, preparation of gel electrolyte by ultrasonic dispersion, filling of gelled-electrolyte in vacuum and long formation time is difficult to be realized for most lead-acid battery manufacturers, and short gel time

* Corresponding author. Tel.: +86 571 87951513; fax: +86 571 87951895.
E-mail address: wjm@zju.edu.cn (J. Wang).

0378-7753/$ – see front matter © 2007 Published by Elsevier B.V.
doi:10.1016/j.jpowsour.2006.12.031

and long stable time of the filled batteries at open-circuit also limit their industrial application. Moreover, a higher iron content and other impurities can decrease the overpotentials for hydrogen and oxygen evolution, and thus greatly increase water consumption in the gel batteries, which leads to battery failure [7,10,14].

Polysiloxane compounds are types of polymer with Si–O bonds in their main chains. Polysiloxane has been widely applied in the field of chemical engineering, e.g., in coatings, textiles, paints and dyeing materials [17–19] because of its advantage in terms of thermal, chemical and mechanical stability. Recently, there have been an increasing number of reports on its application in electrochemical systems (e.g., lithium polymer batteries) due to its high conductivity, good strength and flexibility as solid polymer electrolyte [20–25]. By contrast, few applications in the field of lead-acid batteries as a polyelectrolyte have been reported. In the present work, a mixed polysiloxane gel is used as a new gelling agent for VRLA batteries. Polysiloxane-based gel electrolyte (PBGE) can be prepared by mixing several composites in a high-speed mixer. The manufacturing process is simple, and the prepared PBGE with good fluidity, low viscosity and long gel time (more than 3 h) can be filled into batteries without the need of a vacuum filler. The physicochemical properties of PBGE and the performance of AGM–PBGE hybrid batteries are investigated and compared with those of CSGE and AGM–CSGE batteries.

2. Experimental

2.1. Preparation of gel electrolytes and batteries

The colloid silica gel electrolyte used for the AGM–CSGE batteries was prepared by mixing colloid silica obtained from Shanghai Hersbit Company, water and sulfuric acid ($1.45\,g\,cm^{-3}$) in a high-speed mixer for 20 min at 1500 rpm. The optimized weight ratio of colloid silica, water and sulfuric acid ($1.45\,g\,cm^{-3}$) is 1:2.1:4.35. The calculated concentration of H_2SO_4 in the mixture was about $1.245\,g\,cm^{-3}$.

The mixed polysiloxane gel was prepared as follows. Organically modified polysiloxane (molecular weight < 3000) with hydrophilic groups, methyl silicon oil (viscosity < 1500 P), tetramethoxysilane (TMOS) and de-ionized water were mixed and strongly stirred. The detailed synthesis procedure has been described previously [26,27].

To obtain the best compromise between improvement of the physical properties of PBGE (including an easily controlled gelling time of 3–4 h, good gel thixotropy and strength) and retention of the advantages of AGM batteries, the optimized weight ratio of polysiloxane polymer, water and sulfuric acid ($1.53\,g\,cm^{-3}$) is 1:4.9:6.6. In this case, the calculated concentration of H_2SO_4 is identical to that in the AGM–CSGE batteries before formation.

The AGM–CSGE and AGM–PBGE hybrid batteries, rated as 12 V/75 Ah and 2 V/200 Ah, respectively, were assembled using the same AGM separator and other components, except for the different PBGE and CSGE electrolytes. In order to improve the distribution of the two gel electrolytes between the plates, PBGE and CSGE were filled into the battery cases using a vacuum system. It should be pointed out that in order to promote penetration of silica particles inside the gel plates, the prepared PBGE containing sulfuric acid and polysiloxane-based polymer should be filled into the battery cases in 3–4 h after mixture, and the AGM–PBGE hybrid batteries should be kept at open-circuit for several hours. The CSBE has a short gel time (less than 45 min at 30 °C) and therefore must be filled into the AGM–CSGE batteries within 30 min. The algorithm used for the formation of the AGM–CSGE and AGM–PBGE hybrid batteries was the same as that employed for normal AGM batteries.

2.2. Electrochemical test

Cyclic voltammetry experiments were carried out in PBGE or CSGE using a model 273A poteniostat, and the potential scan was conducted at a rate of $10\,mV\,s^{-1}$ between −1.8 and 1.8 V. A classical three-electrode cell was used. A planar lead alloy (0.9 wt% Sn–0.09 wt% Ca) electrode with an exposed geometric area of $1\,cm^2$ was used as the working electrode. A platinum foil was employed as the counter electrode and a Hg/Hg_2SO_4 electrode as the reference. Electrochemical experiments were conducted at 25 °C, except where otherwise stated.

2.3. Battery test

High-rate discharge and cold-cranking were performed with Digatron UBT series instrumentation. A high- or low-temperature test and a cyclic overdischarge test during partial-state-of-charge (PSoC) cycle-life were performed for the AGM–CSGE and AGM–PBGE hybrid batteries (12 V/75 Ah) by means of Bitrode battery test modules. Details of the cyclic test algorithm are presented in Table 1. Cycle-life testing of the AGM–CSGE and AGM–PBGE hybrid batteries, rated as 2 V/200 Ah (100% DoD), was carried out with an Arbin BT-2000 system. Tests of the oxygen-recombination efficiency and internal resistance of the two hybrid batteries (2 V/200 Ah) were carried out according to the International Electrotechnical Commission (IEC) 60896-2-1 standard.

2.4. Physical characterization

The Fourier transform infrared (FTIR) of the prepared polysiloxane polymer was recorded by means of a Nicolet Nexus

Table 1
Cyclic overdischarge test during partial-state-of-charge (PSoC) cycle-life for AGM–CSGE and AGM–PBGE hybrid batteries (12 V/75 Ah)

Step	Test algorithm
1	Charge or recharge (7.5 A/14.1 V/24 h)
2	Discharge (7.5 A/10.8 V)
3	Rest (5 h)
4	Charge (7.5 A/8 h)
5	Discharge (7.5 A/10.8 V)
6	Cycle from step 3 to step 5 for four times
7	Rest (5 h)
8	Go to step 1 for cycle till 35 times

670 Fourier transform infrared spectrophotometer in a conventional NaCl slice. The morphologies of the samples were observed with a SIRION scanning electron microscopy (SEM, FEI, USA). The two gel electrolytes were sputtered and coated with a thin layer of gold to improve image quality. X-ray diffraction (XRD) analysis was performed using a Rigaku D/Max 2550 X-ray diffractometer fitted with Cu Kα radiation at 40 kV, 300 mA and a scan rate of 1.2° (2θ) min^{-1}.

3. Results and discussion

3.1. Gel electrolyte characterization

The FTIR spectrum of polysiloxane-based polymer is displayed in Fig. 1. The characteristic peaks at 1130, 812 and 475 cm^{-1} may be ascribed to the asymmetrical, symmetrical stretching and bending vibrations of Si–O–Si, respectively [19,28]. This indicates the existence of Si–O–Si bonds in the polysiloxane-based polymer. The two peaks at 1451 and 1380 cm^{-1} are the asymmetrical and symmetrical stretching vibrations of C–H bonds, respectively [28]. There are no peaks representing Si–OH (960 cm^{-1}) and Si–O–Me (2817 cm^{-1}) in Fig. 1. This indicates that the condensation reaction has terminated completely under the present experimental conditions, and the prepared mixed polysiloxane polymer in this system has good chemical stability.

Cyclic voltammetry (CV) curves for the planar lead alloy electrode in PBGE and CSGE systems are presented in Fig. 2. Similar peaks are found in the two CV curves in the potential range of −1.4 to 1.4 V, which implies that the oxidation and reduction processes of lead are similar in the PBGE and CSGE systems. It can be clearly seen from Fig. 2(b and c) that the hydrogen evolution potential in PBGE electrolyte is more negative than that in CSGE and that the oxygen evolution potential is more positive in the polysiloxane-base gel electrolyte. Moreover, the two corresponding peak currents in PBGE electrolyte (peaks A and B) are much lower than those in CSGE system (peaks A′ and B′). These results show that the hydrogen and oxygen evolution reactions are greatly inhibited in the PBGE system,

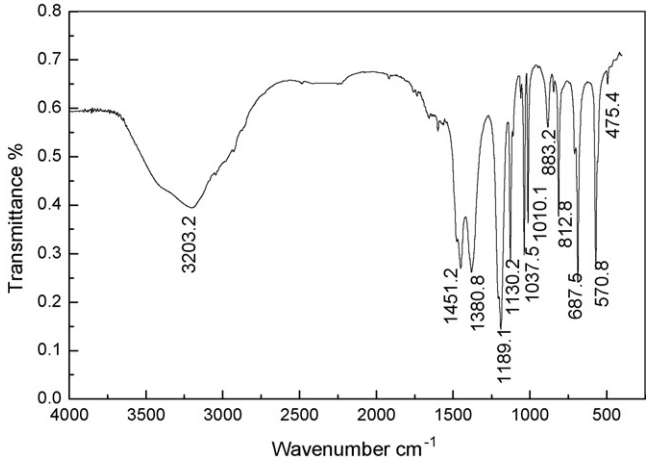

Fig. 1. FTIR spectrum of prepared polysiloxane-based polymer.

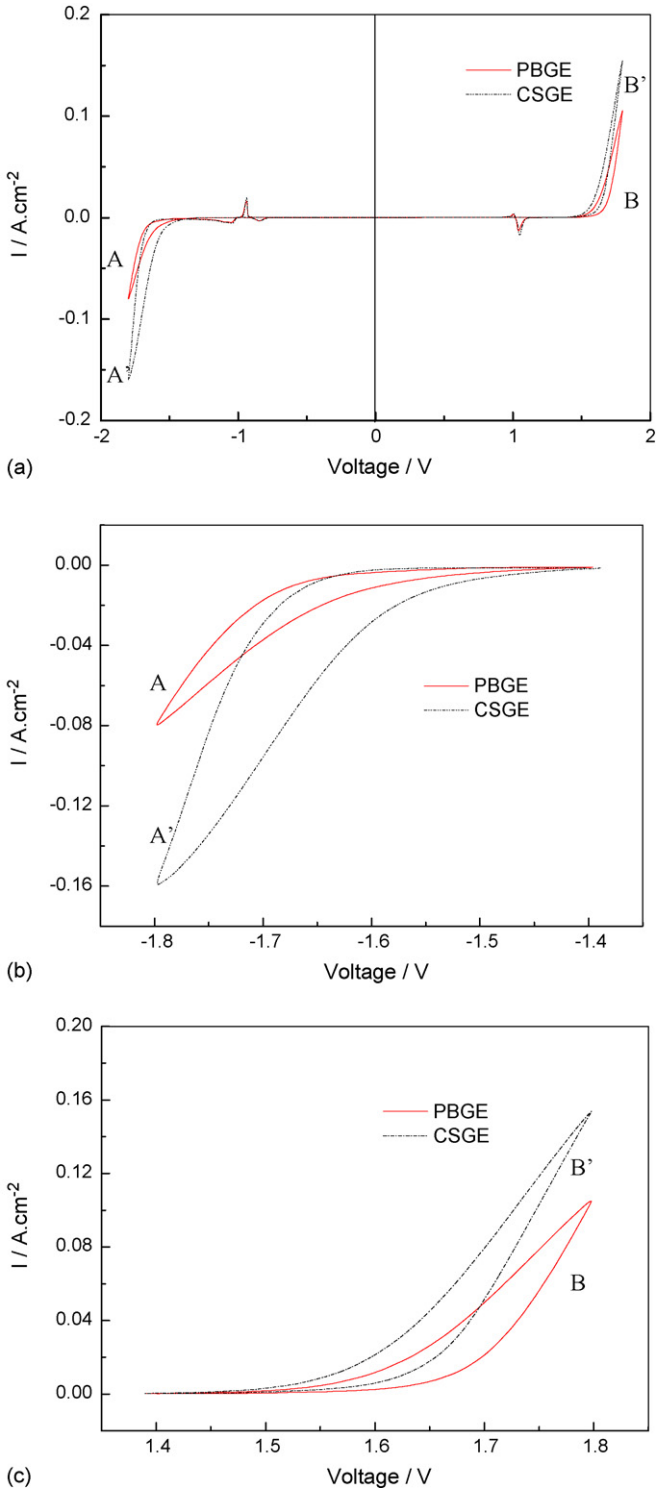

Fig. 2. Cyclic voltammogram curves (a) of lead alloy in PBGE and CSGE electrolytes between −1.8 and 1.8 V at 10 mV s^{-1} and magnified plots of negative-potential (b) and positive-potential (c) regions.

which might result from a relatively low content of impurities such as iron, chloride, etc. in PBGE [12]. This suggests that a lower self-discharge rate, much less water loss and a higher charge efficiency might be expected in PBGE system, that is, the performance of the AGM–PBGE hybrid batteries can be significantly improved. In addition, the CV results shown in Fig. 2,

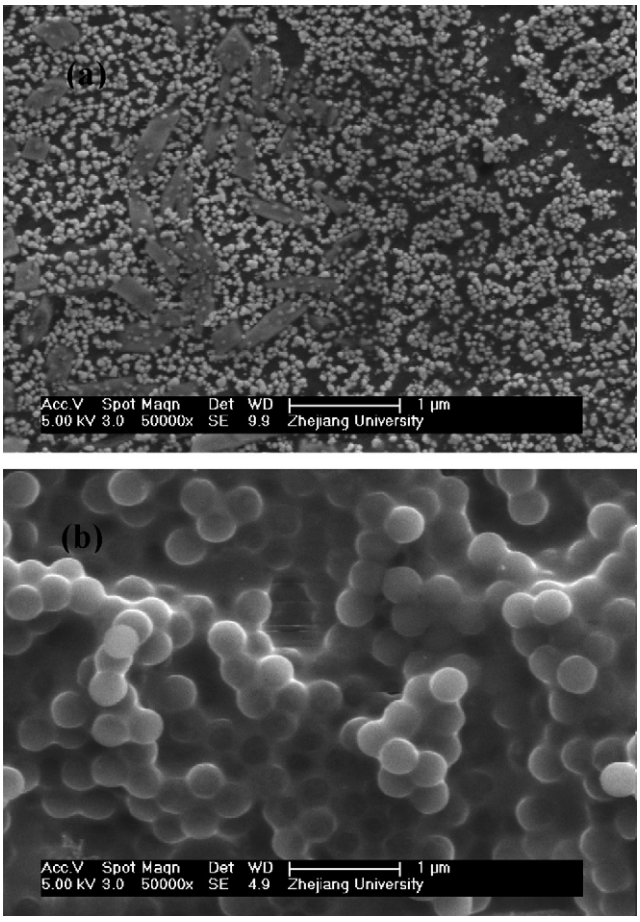

Fig. 3. Scanning electron micrographs of polysiloxane-based polymer before (a) and after (b) gelling with sulfuric acid (1.285 g cm^{-3}) (stored for 1 month).

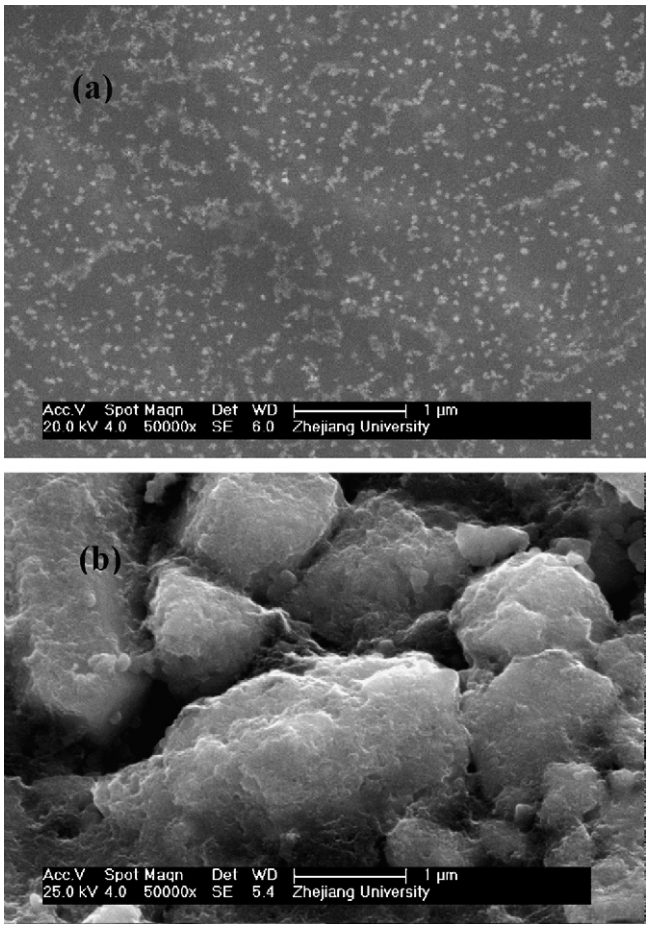

Fig. 4. Scanning electron micrographs of colloid silica electrolyte before (a) and after (b) gelling with sulfuric acid (1.285 g cm^{-3}) (stored for 1 month).

also suggest that PBGE is considerably stable and can be widely used in VRLA batteries.

Scanning electron micrographs of colloidal silica and polysiloxane before and after gelling with sulfuric acid are presented in Figs. 3 and 4, respectively. The micrograph shown in Fig. 3(a) reveals that the morphology of the prepared polysiloxane particles is well formed and predominantly spherical, and that the particle sizes are 30–50 nm. Little aggregation or crosslinking of particles has been observed after storage for 1 month, which indicates the excellent dispersion and stability of the polymer particulates. While Fig. 4(a) shows that colloid silica particles are prone to aggregate and display a non-spherical shape, their particle sizes are similar to those of polysiloxane particles. After gelling with sulfuric acid, polysiloxane-based gel electrolyte (PBGE) displays a three-dimensional network structure due to inter-particle or intra-particle crosslinking, and its particles are spherical in shape, with a diameter of approximate 200 nm (Fig. 3(b)). While CSGE consists of much larger particles (∼1 μm) with irregular shape, and the connections between various particles are poor (Fig. 4(b)), which may be detrimental to the penetration of CSGE inside the batteries [29].

In general, the oxygen-recombination efficiency of common gel batteries is lower than that of AGM batteries in initial period [3,30], because the formation of cracks, which is necessary for oxygen diffusion to negative plates, requires some time. In our work, however, the AGM–PBGE hybrid batteries display a higher oxygen-recombination efficiency (99.5%) than the AGM–CSGE batteries (96.6%) during initial cycle. It should be noticed that the oxygen-recombination efficiency of AGM–PBGE hybrid batteries is almost the same as that of normal AGM batteries. This shows that the three-dimensional network structure of PBGE facilitates the formation of micropores in the AGM separator, and then enhances the diffusion and recombination of oxygen.

3.2. Battery test

The usage of gel electrolytes in VRLA batteries usually results in an increase of internal resistance, and this can deteriorate the discharge performance of the batteries (especially the high-rate discharge performance) due to an increase in electrode polarization [9,10,15]. In our study, however, the internal resistances of AGM–CSGE, AGM–PBGE and normal AGM batteries (2 V/200 Ah) are 0.776, 0.656 and 0.674 mΩ, respectively. This shows that the usage of PBGE does not result in an increase of internal resistance; on the contrary, a slight decrease in internal resistance is observed. Therefore, the AGM–PBGE hybrid batteries present higher discharge voltage and larger

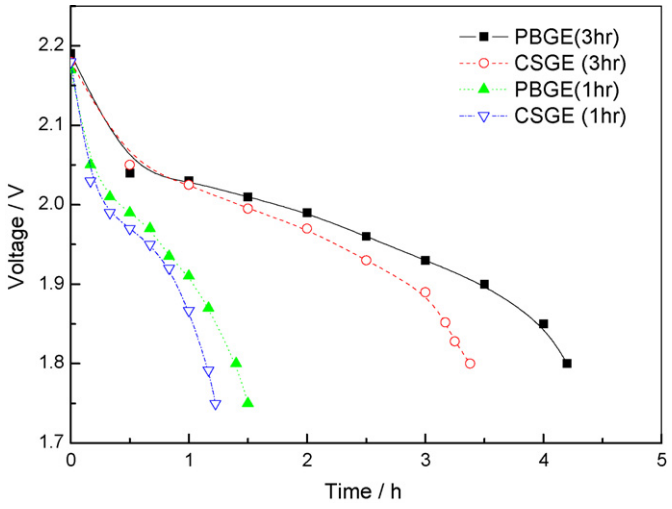

Fig. 5. Initial discharge curves for AGM–PBGE and AGM–CSGE hybrid batteries (2 V/200 Ah) at 3-h rate and 1-h rate.

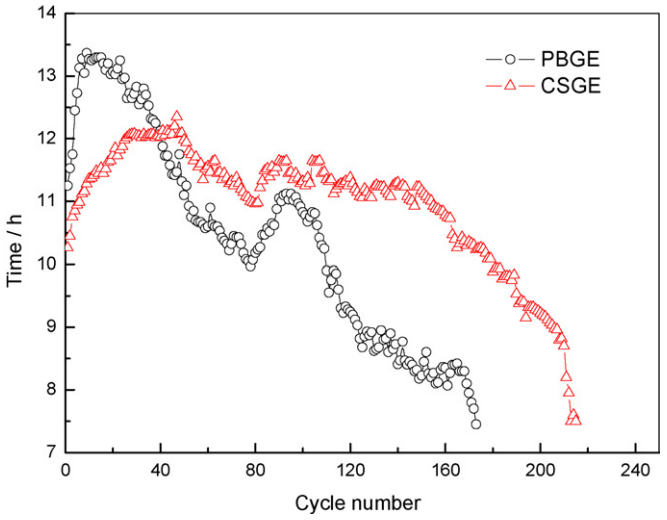

Fig. 7. Cycle-life curves of AGM–PBGE and AGM–CSGE hybrid batteries (2 V/200 Ah) at 100% DoD at 10-h rate.

discharge capacity than the AGM–CSGE ones, especially at relatively high-rates (Figs. 5 and 6). The micropores in PBGE electrolyte may provide a pathway for diffusion of reactive species and, accordingly, enhance the transfer of reactive species between the positive and negative plates. Thus, the concentration polarization during charge and discharge is reduced. This might be responsible for the superior rate capability of AGM–PBGE hybrid batteries.

The cyclic performance of the two hybrid batteries (2 V/200 Ah) at the 10-h rate under a condition of 100% DoD is illustrated in Fig. 7. The two hybrid batteries display a similar variation trend in cyclic performance, that is to say, as the electrochemical cycling proceeds, their discharge capacities first increase, and then decrease gradually. The increase of discharge capacity during initial cycles may result from the penetration of gel electrolytes inside batteries, the formation of cracks or micropores for the diffusion of reactive species, and the activation of active materials. The decrease in discharge capacity after certain cycles might originate from destruction of the electrode structure. The three-dimensional network structure with the relatively small particle size of PBGE facilitates its penetration inside the batteries and the formation of transfer paths for reactive species. Hence, the AGM–PBGE hybrid batteries display a faster rise in discharge time and a larger discharge capacity during initial cycles, compared with AGM–CSGE hybrid batteries. The relatively faster decline in discharge capacity after about 20 cycles indicates that the inside structure of AGM–PBGE hybrid batteries has a larger deterioration rate than that of AGM–CSGE hybrid batteries under the present charge–discharge conditions (0.1 C, 2.35 V/cell for 24 h, 100% DoD).

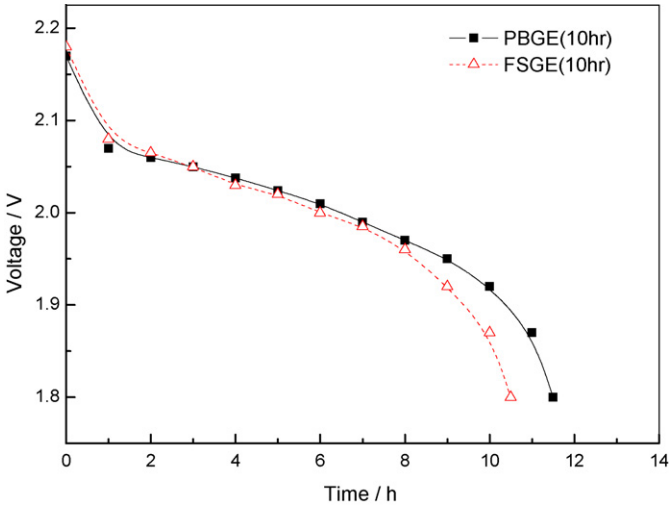

Fig. 6. Initial discharge curves for AGM–PBGE and AGM–CSGE hybrid batteries (2 V/200 Ah) at 10-h rate.

In order to investigate the recharge and discharge properties of the two batteries under overdischarge conditions, the electrochemical performance of AGM–PBGE hybrid and AGM–CSGE batteries during PSoC cycling has been tested according to the rules given in Table 1. The results are described in Fig. 8. The AGM–PBGE hybrid batteries in a full-charge state and PSoC display much larger discharge capacity and better cyclic stability than the AGM–CSGE counterparts. This suggests that the former batteries have better recharge and discharge performance under the overdischarge conditions. This may be attributed to greater charge efficiency resulting from the increase in hydrogen and oxygen evolution overpotentials, good conductivity and the open three-dimensional network structure of PBGE.

After the PBGE and CSGE hybrid batteries (2 V/200 Ah) had been fully charged for 24 h during current-limited constant-voltage step (0.1 C, 2.35 V/cell), their discharge performance at different temperatures was evaluated. The AGM–PBGE batteries present longer discharge time in the temperature range of −40 to 50 °C, and the increase in discharge time is more obvious in the two temperature ranges of −40 to −10 and 10–50 °C (Fig. 9). The AGM–PBGE batteries display higher discharge voltage and much longer discharge time than the AGM–CSGE batteries at −40 °C (Fig. 10). Moreover, it is found that the discharge time of the AGM–PBGE batteries, rated as 12 V/75 Ah under the conditions of −18 °C, 650 A discharge rate and 9.6 V cut-off voltage,

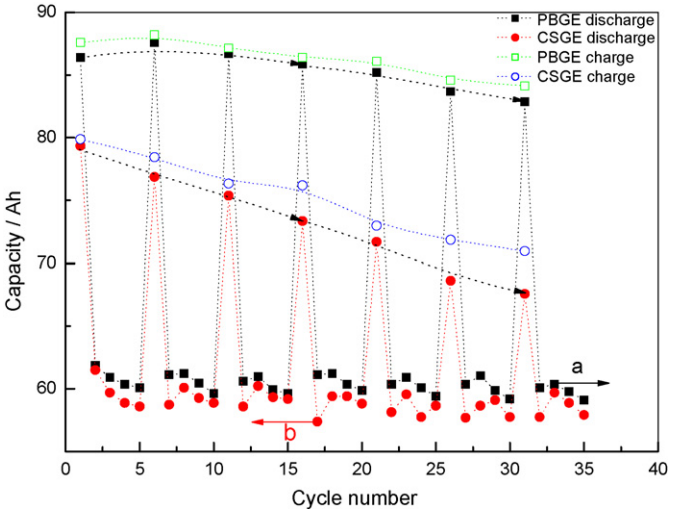

Fig. 8. Cyclic overdischarge test during PSoC cycle-life of AGM–PBGE and AGM–CSGE hybrid batteries (12 V/75 Ah, discharged at 10-h rate). Curves (a and b)—discharge capacity for AGM–PBGE and AGM–CSGE hybrid batteries after insufficient charging, respectively.

is 42 s, which is 4.8 times greater than that of the AGM–CSGE batteries. The above results show that the AGM–PBGE batteries have superior high- and low-temperature performance, implying that PBGE is also stable at higher and lower temperatures.

3.3. Failure mode comparison

Measurements of the potentials of the positive and negative plates during discharge tests of AGM–PBGE and AGM–CSGE batteries that have failed after deep-discharge cycling (100% DoD) show that, in both cases, failure results mainly from degradation of their respective positive plates. Therefore, the microstructure and phase composition of the positive active material (PAM) before cycling and after failure are investigated in the following sections.

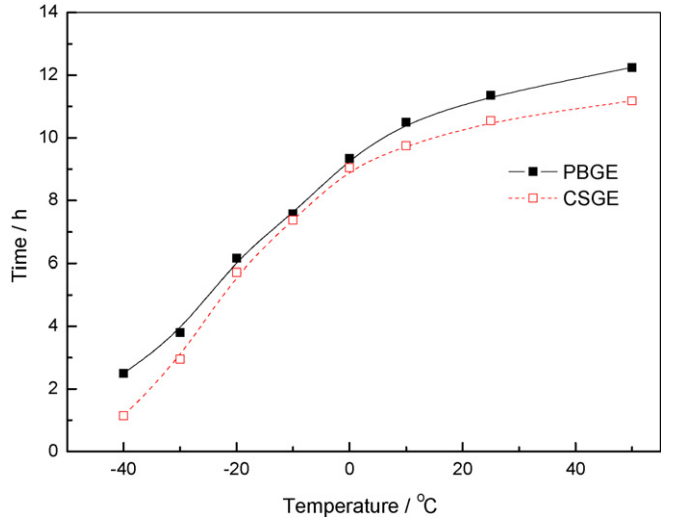

Fig. 9. Discharge vs. time comparison of AGM–PBGE and AGM–CSGE hybrid batteries at different temperatures (2 V/200 Ah, discharged at 10-h rate).

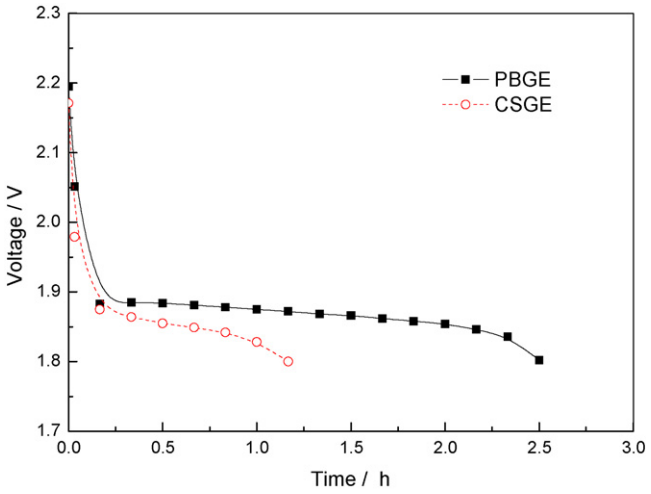

Fig. 10. Discharged voltage vs. time of AGM–PBGE and AGM–CSGE hybrid batteries at −40 °C (2 V/200 Ah, discharged at 10-h rate).

3.3.1. SEM analysis of PAM

Scanning electron micrographs of the PAM in fully charged AGM–PBGE and AGM–CSGE hybrid batteries before cycling and after failure are presented in Figs. 11 and 12, respectively. The PAM in both batteries consists of a large amount

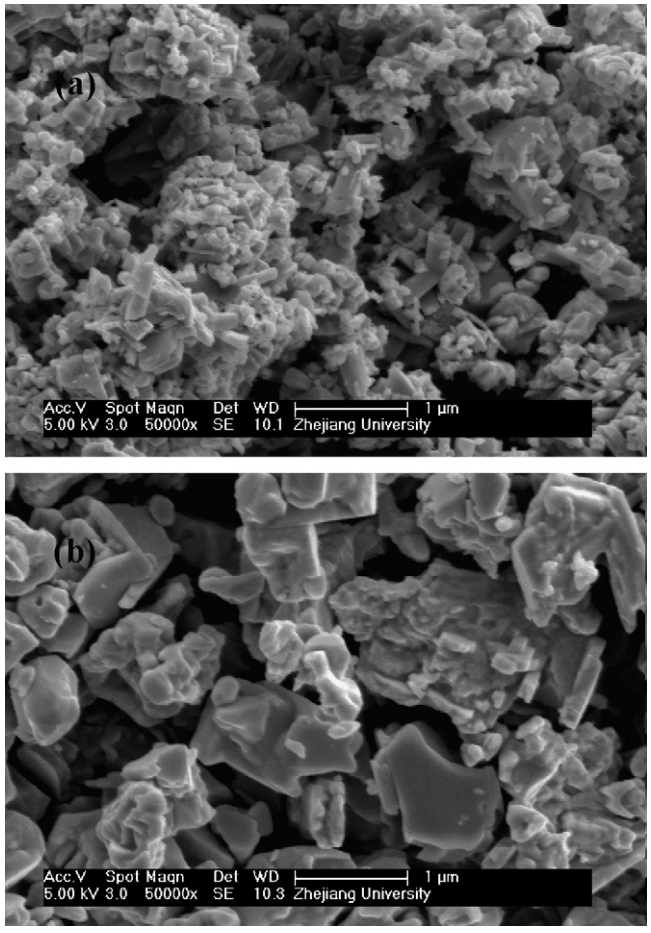

Fig. 11. Scanning electron micrographs of PAM in AGM–PBGE hybrid batteries: (a) before cycling and (b) after failure.

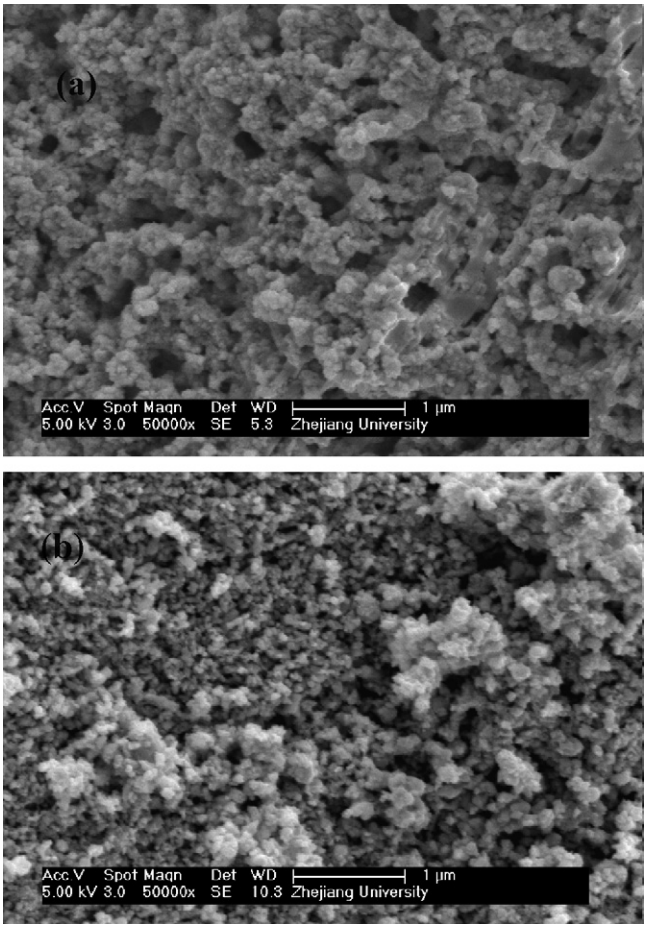

Fig. 12. Scanning electron micrographs of PAM in AGM–CSGE hybrid batteries: (a) before cycling and (b) after failure.

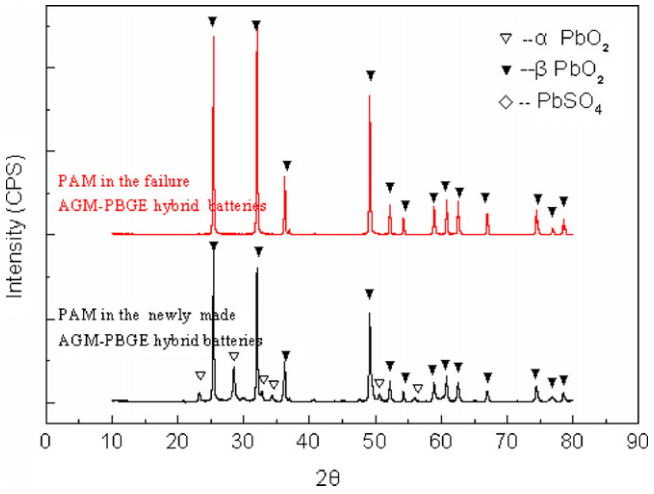

Fig. 13. X-ray diffraction patterns of PAM in fully charged state in AGM–PBGE hybrid batteries before cycling and after failure.

of small grains with irregular shape and a lesser amount of large grains with a polyhedral shape before electrochemical cycling. It is noted from Figs. 11(a) and 12(a) that the initial PAM in AGM–PBGE hybrid batteries displays a more porous structure than that in AGM–CSGE hybrid batteries. This results from the formation of an open three-dimensional network structure due to the penetration of polysiloxane-based particles in the plates. Thus, a strong and open skeleton is formed, which is beneficial for improving access of reactive species such as H_2O and H_2SO_4 to the inside of the PAM. This may be one of main reasons for the enhanced utilization of PAM and the improved high-rate discharge performance of the PBGE system. During disassembly of the failed batteries, however, it is found that the contact between the PAM and the grid, as well as between the individual PAM aggregates, in any portion of the two hybrid batteries plates is very loose, which is not a universal phenomenon in AGM batteries that have undergone normal failure. The phenomenon is more remarkable at the bottom of the PBGE plates. This may be evidence of the better penetration of polysiloxane-based particles and higher utilization of PAM in the plates. Fig. 11(b) indicates that the failed PAM in AGM–PBGE hybrid batteries consists mainly of large grains with a polyhedral shape and that the positive plates become looser and less porous. In addition, serious aggregation of PAM grains occurs. This greatly reduces the effective surface area of the positive plates and this may be partially responsible for failure of the batteries. Furthermore, the weakening of the gel strength with cycling may cause gradual disruption of the three-dimensional network structure, which can accelerate softening and shedding of the PAM. As a consequence, the AGM–PBGE hybrid batteries begin to fail. For AGM–CSGE failure batteries, softening and shedding of PAM in the plates also occur. As shown in Fig. 12(b), however, the particles of PAM become much smaller due to the pulverization of some particles. Accordingly, connections between various particles become very poor and the network structure of PAM nearly disappears, which results poor electrical connection of zones in PAM [31].

Chemical analysis of PAMs shows that more than 94% PbO_2 remains in the positive plates of the two failed hybrid batteries when in a fully charged state. This further indicates that the loss of contact resulting from PAM expansion and the phase composition change are responsible for failure of the two batteries, rather than the change in PAM content.

3.3.2. XRD analysis

X-ray diffraction patterns of PAM in the fully charged state in AGM–PBGE and AGM–CSGE hybrid batteries before cycling and after failure are given in Figs. 13 and 14, respectively. Before cycling, the PAM in the AGM–PBGE batteries consists of mainly a large amount of β-PbO_2 and some of α-PbO_2, whereas the PAM in the AGM–CSGE hybrid batteries contains a large quantity of β-PbO_2, some α-PbO_2 and a small amount of $PbSO_4$ that results from an insufficient formation time. The existence of $PbSO_4$ might be partially responsible for low initial capacity of AGM–CSGE hybrid batteries, as shown in Fig. 7. During the electrochemical cycling of AGM–CSGE batteries, the $PbSO_4$ crystals may be gradually converted to PbO_2 crystals and these may make a contribution to the increase in the discharge capacity of the batteries after 50 cycles.

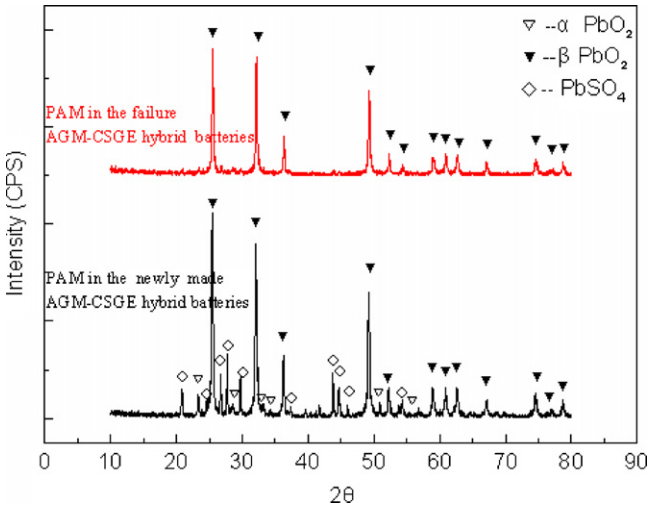

Fig. 14. X-ray diffraction patterns of PAM in fully charged state in AGM–CSGE hybrid batteries before cycling and after failure.

It is noted from Figs. 13 and 14 that after failure, the PAM in fully charged hybrid batteries consists only of β-PbO_2. This indicates that the α-PbO_2 in the original PAM of the two hybrid batteries and the $PbSO_4$ in initial CSGE plates have been fully transformed into β-PbO_2 after undergoing electrochemical cycling. The data in Fig. 7 imply that the conversion rate in AGM–PBGE hybrid batteries may be faster than that in the AGM–CSGE hybrid counterparts. This may be because PBGE with the three-dimensional network structure and relatively small particle size provides better penetrationability of the electrolyte. With the conversion of α-PbO_2 to β-PbO_2 during electrochemical cycling, the content of α-PbO_2 in the two batteries gradually decreases and finally disappears. This results in the positive plates undergoing a capacity loss during cycling due to [32,33] an increase in the particle size of the PAM aggregates (as shown in Fig. 11) and in the loss of structural water, as well as poor contact between the PAM particles (as shown in Figs. 11 and 12). Hence, there is softening and shedding of the PAM, which leads to the failure of the two hybrid batteries.

The Rietveld full-profile fitting method [34] was used for the XRD quantitative analysis of PbO_2 and $PbSO_4$ crystals in the PAM. The results show that the ratio of $\beta/(\alpha+\beta+PbSO_4)$ in the PAM of AGM–PBGE and AGM–CSGE hybrid batteries before cycling is 0.644 and 0.556, respectively. Since β-PbO_2 has a higher electrochemical activity than α-PbO_2 [35], the AGM–PBGE batteries with a relatively high β-PbO_2 content exhibit a better initial electrochemical performance.

4. Conclusions

Compared with AGM–CSGE batteries, AGM–PBGE batteries display: (i) superior initial electrochemical performance, especially at higher discharge rate; (ii) improved low- and high-temperature properties; (iii) better recharge and discharge performance under overcharging conditions. On the other hand, the AGM–CSGE batteries give a poorer cycle performance at the 10-h rate under the condition of 100% DoD. The improved performance of the AGM–PBGE hybrid batteries results mainly from an increases in both the hydrogen and oxygen evolution overpotentials, good conductivity with lower internal resistance and an open three-dimensional network structure with PBGE of a relatively small particle size. It is found that the softening and shedding of the PAM are mainly responsible for the failure of AGM–PBGE and AGM–CSGE hybrid batteries.

Acknowledgements

The authors are grateful to the R&D centre in Zhejiang Narada Power Source Co., Ltd., for supporting part of this research. Thanks are also due to Prof. J.Y. Wang for his helpful suggestions. Finally, the authors acknowledge the financial support from the Chinese State Key Laboratory for Corrosion and Protection.

References

[1] H. Tuphorn, J. Power Sources 46 (1993) 361–373.
[2] G. Posch, J. Power Sources 33 (1991) 127–133.
[3] H. Tuphorn, J. Power Sources 40 (1992) 47–61.
[4] M.P. Vinod, K. Vijayamohanan, J. Appl. Electrochem. 24 (1994) 44–51.
[5] M.P. Vinod, K. Vijayamohanan, J. Appl. Electrochem. 25 (1995) 80–87.
[6] M.P. Vinod, K.B. Mandle, S.R. Sainkar, K. Vijayamohanan, J. Appl. Electrochem. 27 (1997) 462–468.
[7] M.P. Vinod, K. Vijayamohanan, S.N. Joshi, J. Power Sources 70 (1998) 103–105.
[8] M.P. Vinod, K. Vijayamohanan, J. Power Sources 89 (2000) 88–92.
[9] L. Wu, H.Y. Chen, X. Jiang, J. Power Sources 107 (2002) 162–166.
[10] D.W.H. Lambert, P.H.J. Greenwood, M.C. Reed, J. Power Sources 107 (2002) 173–179.
[11] K.R. Bullock, J. Power Sources 116 (2003) 8–13.
[12] S.K. Martha, B. Hariprakash, S.A. Gaffoor, S. Ambalavanan, A.K. Shukla, J. Power Sources 114 (2005) 560–567.
[13] J. Park, S.B. Park, S.M. Yang, W.H. Hong, C.R. Choi, J.H. Kim, J. Non-Cryst. Solids 351 (2005) 2352–2357.
[14] J.C. Hernandez, M.L. Soria, M. Gonzalez, E. Garcia-Quismondo, A. Munoz, F. Trinidad, J. Power Sources 162 (2006) 851–863.
[15] E. Nann, J. Ruch, US Patent 6,635,386 (2003).
[16] D. Bechtold, J. Vollbert, US Patent 5,338,596 (1994).
[17] H.L. Li, Y. Ujihira, T. Yoshino, K. Yoshii, T. Yamashita, K. Horie, Polymer 39 (1998) 4075–4079.
[18] N. Furukawa, M. Yuasa, Y. Kimura, Polymer 40 (1999) 1853–1862.
[19] Y. Kaneko, N. Iyi, T. Matsumoto, K. Kitamura, Polymer 46 (2005) 1828–1833.
[20] Z.W. Zhang, C.K. Park, L.Y. Sun, C. Chai, US Patent 6,547,839 (2003).
[21] R.C. West, Z.C. Zhang, US Patent 6,887,619 (2005).
[22] Z.C. Zhang, L.J. Lyons, K. Amine, R. West, Macromolecules 38 (2005) 5714–5720.
[23] I.J. Lee, G.S. Song, W.S. Lee, D.H. Suh, J. Power Sources 114 (2003) 320–329.
[24] Y. Kang, J. Lee, D.H. Suh, C. Lee, J. Power Sources 146 (2005) 3910–3916.
[25] P. Taranekar, X.W. Fan, R. Advincula, Langmuir 18 (2002) 7943–7952.
[26] S.Q. Dong, C.S. Nie, CN Patent 1663984A, 2004.
[27] Y.R. Liu, Y.S. Feng, CN Patent 1312331A, 2002.
[28] S.Y. Feng, J. Zhang, M.J. Li, Q.Z. Zhu, Organic Silicon Polymer and its Application, China Chemical Industry Press, Beijing, 2004, pp. 414–420.
[29] C. Linder, M. Nemas, M. Perry, R. Katraro,US Patent 5,265,734 (1993).
[30] J. Kwasnik, J.D. Milewski, T. Pukacka, B. Szczesniak, J. Power Sources 42 (1993) 165–171.

[31] M. Calabek, K. Micka, P. Bala, J. Power Sources 62 (1996) 161–171.
[32] I. Petersson, E. Ahlberg, B. Berghult, J. Power Sources 76 (1998) 98–105.
[33] P.D. Xu, H.T. Liu, Lead Acid Batteries-Basic Theory and Techniques, Shanghai Press of Science and Technology, Shanghai, China, 1993, pp. 139–199.
[34] D.L. Bish, J.E. Post, Quantitative Mineralogical Analysis Using the Rietveld Full-Pattern Fitting Method, Press of American Mineralogist, New York, 1993, pp. 932–940.
[35] P.K. Shen, X.L. Wei, Electrochim. Acta. 48 (2003) 1743–1747.